Exp Fluids (2017) 58:38
DOI 10.1007/s00348-017-2311-4

RESEARCH ARTICLE

Schlieren technique in soap film flows

M. I. Auliel[1] · F. Castro Hebrero[1] · R. Sosa[1] · G. Artana[1]

Received: 30 June 2016 / Revised: 2 February 2017 / Accepted: 3 February 2017

Abstract We propose the use of the Schlieren technique as a tool to analyse the flows in soap film tunnels. The technique enables to visualize perturbations of the film produced by the interposition of an object in the flow. The variations of intensity of the image are produced as a consequence of the deviations of the light beam traversing the deformed surfaces of the film. The quality of the Schlieren image is compared to images produced by the conventional interferometric technique. The analysis of Schlieren images of a cylinder wake flow indicates that this technique enables an easy visualization of vortex centers. Post-processing of series of two successive images of a grid turbulent flow with a dense motion estimator is used to derive the velocity fields. The results obtained with this self-seeded flow show good agreement with the statistical properties of the 2D turbulent flows reported on the literature.

1 Introduction

Efforts to develop high-quality techniques of flow visualization date from a long time ago. Dye injection at some points of the flow has been one of the most traditional approaches to visualize the locus of points of the fluid particles that have passed through the same dye injection point (streak-lines). The inspection of the recorded images has normally aimed at an interpretation of these streak-lines to lend an overall global insight into the flow properties, by taking advantage of the pattern recognition capabilities of the naked eye. An underlying hypothesis of the streak-line analysis is that the motion of the dye particles (tracers) follow the motion of the neighbouring fluid and that diffusion of the dye is not significant.

Since the pioneering works of Couder et al. (1989) and Kellay et al. (1995), soap films stretched between two wires and flowing under gravity have raised the interest of different researchers. The interposition of an obstacle in the free flow produces a redistribution of velocity and pressure that perturbs the film thickness a phenomenon that can be used to obtain high quality visualizations of the flow. Under controlled experimental conditions the soap film flows are expected to be quasi two-dimensional (2D). Hence, soap film tunnels are attractive experimental platforms to perform studies to understand the underlying physics of flows that appear for instance in the oceanography or meteorological domain.

The analysis of the patterns of images of the flowing soap film differs from the traditional streak-line analysis, as the flow visualization in soap films does not involve any external tracer and the structures observed are related to the instantaneous thickness field. The techniques used for visualization of the flow patterns in soap films rely on optical methods that make the thickness variations evident.

1.1 Visualization techniques

1.1.1 Interferometric technique

The standard technique to observe the patterns dynamics is the interferometric technique that consists in the illumination of the sheet with a monochromatic light at an angle of incidence and the recording of the reflected image. The image is formed thanks to a phase shift of the

✉ M. I. Auliel
mauliel@fi.uba.ar

[1] Laboratorio de Fluidodinámica, Facultad de Ingeniería, Universidad de Buenos Aires, CONICET, Av. Paseo Colón 850, C1063ACV Buenos Aires, Argentina

Published online: 03 April 2017

electromagnetic wave produced by the fluid. The reflection from the front and rear surfaces of the film creates interference fringes that are a function of the local value of the film thickness. When white light is used, the cumulative effect of the interference from each wavelength constituting the white light gives rise to patterns with different colours. Thus, the thickness variations over the whole film, can be mapped from the coloured fringes observed in the film. The interpretation of the thickness patterns as an equivalent feature of a 2D general flow is not straightforward. Yang et al. (2001) observed that the colour fringes appearing in soap films may resemble streamlines for steady 2D flows. In the non steady cases, and under experimental conditions that depend on the flow velocities and on the liquid solution properties, the dynamics of the fringe patterns have also been associated by other researchers to the dynamics of pressure fields of vorticity fields, or to the dynamics of advected passive scalars (Rivera and Wu 2002). In a recent paper (Auliel et al. 2015), we have analysed this aspect and a synthesis of our results is described in another section of this manuscript.

1.1.2 Using Schlieren as an alternative technique

The simplicity of the interferometry technique compared to other flow visualization techniques that could rely on light deviations by the deformed surfaces of the film, like shadowgraph or Schlieren technique (Settles 2001; Zhong and Jun 2005), has probably retarded the use of such techniques in soap film studies. These techniques are optical methods frequently used for general flow visualization of moving transparent media with mass density variations (Settles 2001; Goldstein 1996). In these flows, the images are produced using collimated light whose optical path is disturbed by changes in the refractive index of the medium traversed by the light. The link between the local refraction index of the media and the local mass density alterations is described in general by the Gladstone–Dale relation. One of the characteristics of the images produced is that the contrast is proportional to a line-of-sight integration of the first spatial derivative (Schlieren) or of the second derivative (shadowgraph) of the refractive index. The techniques may enable the derivation of the whole density field and when the flows under study are two-dimensional (or with axial symmetry) only one image should suffice to obtain the required field. On the other hand, when the flow under consideration is three-dimensional, multiple projections are required in conjunction with the use of tomographic reconstruction techniques (Cabaleiro 2013).

In the case of soap films, the principle of the Schlieren image technique does not actually rely on alterations of mass density but on the different optical paths of initial parallel rays of light traversing the surfaces of the film. The local variations of the thickness of a perturbed film modifies the smoothness of the interfaces that produces deviation of the rays altering the background "unperturbed" image.

1.2 Measurement techniques

1.2.1 Thickness measurements techniques

In soap films flows, as thickness variations are related to flow field dynamics, there have been different efforts to measure the thickness dynamics. Measurements of the local thickness fluctuations in single points have been obtained with a Mach-Zender interferometer. This apparatus uses two parallel beams: a reference beam and a probe beam created from the same HeNe laser (Greffier et al. 2002). This kind of measurement gives good temporal resolution, but the temporal series concern only the position where the probe is placed. Vorobieff et al. (2001) introduced also a method to obtain the thickness field by seeding the film with titanium dioxide particles having a characteristic size 0.2 μm. He proposed to find the local values of the thickness of the film by averaging the intensity of light scattered by the seeding particles. The illumination was performed with a flash lamp and the calibration of the method showed an uncertainty close to 20%. However, the theoretical aspects on which the method is based are not described by the authors (Vorobieff et al. 2001). Tran et al. (2009) have also reported measurements of the thickness of the film using a solution of soap, water and a fluorescent dye. The focusing of a laser beam on a spot of the film made it possible to fluoresce small regions of the fluid that the authors monitored with a photodetector with a counting rate proportional to the thickness.

1.2.2 Velocimetry in soap films

In soap film flows, velocimetry has been usually proposed with the use of seeding particles incorporated to the solution. Different reports of results can be found using LDV apparatus (Kellay et al. 1998; Amarouchene and Kellay 2004; Belmonte et al. 2000; Huang et al. 2004; Samanta et al. 2014), particle tracking or particle image velocimetry (PIV) (Vorobieff et al. 2001; Rivera et al. 1998, 2014; Rivera and Wu 2000; Daniel and Rutgers 2002). Other methods like homodyne photon correlation spectroscopy (HCS) and optical fibre velocimetry (OFV) have also been considered by different researchers (Kellay et al. 1995; Rutgers et al. 1996; Tong et al. 1988; Rivera et al. 1998).

An inherent underlying hypothesis of the use of most of these techniques is that seeding particles behave as a fluid particle of the flow (with no slip or no time lag) and that the added element to the soap solution does not

significantly modify the mechanical aspects of the film behaviour or the surfactant chemical equilibria. Therefore, it is attractive to consider techniques that may circumvent these limitations.

1.2.3 Velocimetry with Schlieren images

The post-processing of the raw Schlieren images of general 3D flows can be applied to obtain the density field of a fluid (Cabaleiro 2013) but also seems a promissory technique to extract relevant and quantitative information of velocity fields. For instance, when air flows are turbulent and the eddies have an intensity strong enough they produce alterations of pressure and therefore of mass density, that may be detected with a Schlieren set up. In these situations no external tracers are required to be incorporated to the flow as it becomes self-seeded by these structures. Thus, velocimetry can be performed trying to determine the motion of these photometric patterns in successive image sequences. To process the Schlieren images of 3D fluid flows, different classical motion estimation methods based on the brightness consistency assumption (correlation-based approaches, optical flow methods) (Settles 2001; Wu et al. 2000; Jonassen et al. 2006; Hargather et al. 2011) or in specific dense motion estimators dedicated to Schlieren images (Sosa et al. 2006; Wang et al. 2015) have been proposed in the past. However, these approaches have been restricted to analyse 3D flows with non-uniform mass density fields and not applied to soap film flows. A discussion of this quantitative analysis with unseeded Schlieren images of soap film flows is, to the best of our knowledge, missing.

1.3 Goals

In this work, we propose to analyse the flow visualizations characteristics provided by the Schlieren technique when applied to flowing soap films and the possibility to perform velocimetry analysis with them. Also, as we illustrate in this manuscript, the images produced with Schlieren technique and with the traditional interferometry technique, produce patterns that are not coincident. Therefore, we propose to compare the characteristics of both kind of images and discuss the advantages of the use of each technique for quantitative purposes of the flow.

The article is organized as follows: in the next section we recall some of the fundamentals of Schlieren techniques, soap film dynamics and dense motion estimators. The third section of the manuscript explains the experimental setup we used and in a fourth section we show visualizations and velocimetry results with both techniques. In a final section, we summarize the results of our work.

2 Fundamentals

2.1 Schlieren imagery in soap films

A Schlieren system is basically a device that produces an image in a screen or in the CCD of a video camera formed as a consequence of the light deviations of parallel beam traversing a transparent fluid (Settles 2001). In the traditional use of Schlieren technique in fluid mechanics, the light beam deviations occurs as a consequence of mass density variations related to the fluid motion.

However, Schlieren system can be proposed to visualize fluid flows even when the origin of deviations in the optical path are not the mass density variations. The technique makes possible for instance to visualize the perturbations of the surface of a flowing film produced by the interposition of an obstacle. The variations of intensity of the image are in this case a consequence of the change of directions of the light beam traversing the deformed surfaces of the film. To the best of our knowledge, this is one of the first works that reports the use of Schlieren in soap film tunnels. We could find only some previous works with a similar setup but without the use of razors blades at the focus position (shadowgraph configuration) applied to the analysis of heated films (Zhong and Jun 2005).

Let us analyse a film of thickness $2H$ with the normal of the unperturbed surface coincident with the direction of the parallel beams. Assuming no density gradients of the surrounding air or in the bulk of the homogeneous film no ray deviation occurs in these regions. So, we consider a case in which the light deviations occur only at the interfaces by the refraction and reflections of the beam. Figure 1 shows a scheme of the optical paths of the rays through the soap film when symmetric perturbations

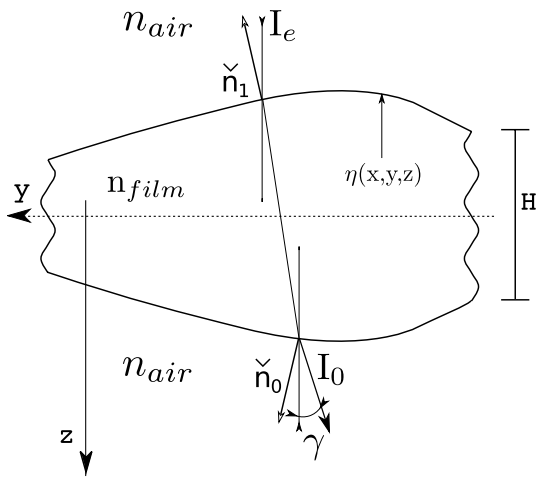

Fig. 1 Soap film considering symmetric perturbations

of the interfaces occur, as this is the most recurrent case of surface deformation for flowing soap films (Chomaz 2001).

The incoming ray, originally parallel to the z axis (I_e), is deviated by two successive refractions to an angle γ.

To simplify the analysis, we show in Fig. 1 a ray deflection only in the y direction (resulting from a surface deformation only function of y). A generalization for any surface deformation that depends on both directions, x and y, is quite straightforward.

With simple optics geometrics, using *Snell's law* and assuming small surface deformations the deflected angle (γ) can be calculated as:

$$\gamma = 2|\nabla\eta|(\mu - 1), \tag{1}$$

As we are considering only a surface deformation on the y direction, we can express

$$\gamma = 2\frac{\partial\eta}{\partial y}(\mu - 1) \tag{2}$$

where μ denotes the ratio of index of refraction (the index of refraction of the soap solution (n_{soap}) divided by the air index of refraction (n_{air})) and η the surface displacement with respect to the unperturbed film thickness H (see Fig. 1).

Thus, the observed light pattern in the Schlieren system is directly related to the components of the gradient of the film thickness. Note that there may exist a contribution to the transmitted light given by secondary reflections of the primary beams on the surfaces. However, the secondary beams that undergo two reflections in the film have an intensity that is at least one order of magnitude lesser than the one transmitted without reflections (Isenberg 1992). Hence, the omission of this effect in the analysis seems adequate.

2.2 Fundamentals of soap film flow dynamics

The flowing soap film can be considered as composed by two thin external layers of surfactants in contact with atmospheric air and a slab of surfactant solution in between. The flux of soap molecules from the bulk to the surface is usually described as an adsorption–desorption process. At the places of the interface where the surfactant is close packed, a desorption occurs from the surface to the bulk phase as well as a spreading towards places of the surface with lower surfactant concentration. At places of the surface with low packed surfactant, adsorption from the bulk takes place, or surface diffusion tends to equilibrate concentrations. The local values of concentration of surfactant at the interface and at the bulk, depend on this advection–diffusion process being both linked through the local flux. For a fully insoluble surface-active substance this flux is null. As the diffusion processes are usually slow, they are customarily disregarded because of the involved time constants. Other effects as evaporation processes may be included in the analysis but their incidence on equilibria is expected to be small.

The vertical film is driven by gravitational forces and the friction forces with the fixed boundaries (usually nylon threads) and the shear with the surrounding air opposes to the flow. The fluid motion of the bulk of the film is described by the 3D incompressible Navier–Stokes equation with the restrictions imposed at the boundaries. The coupling with the air motion makes the problem more complex and simplification of the problem in many cases are proposed by incorporating this effect with an extra term in the momentum conservation equation of the film (Chomaz 2001). Setting this problem apart, the outstanding characteristic of the flow of a soap film is that the motion occurs mainly in the plane of the sheet and that is largely influenced by surface tension forces whose local value depends on the concentration and on the gradients of concentrations of surfactant at the interface. The complexity of the problem arises as the dynamics of the fluid motion, bulk and surface soap concentration equilibriums are largely coupled phenomena. A major issue is to develop the physical and mathematical models capable to describe the coupling of hydrodynamic to surface forces. Three non-dimensional parameters (Re, M_e, Υ) appear in the analysis of this complex kind of flows. The Reynolds number definition $Re = UL/\eta_T$ includes the characteristic length (L) the characteristic velocity of the flow (U) and an effective viscosity (η_T). This effective viscosity takes into account a surface shear viscosity generated by the adsorbed surfactant. It can be evaluated with the Trapeznikov's expression (Trapeznikov 1957) $\eta_T = \eta_b + 2\eta_{int}/H$, (with η_b viscosity of the bulk fluid and η_{int} surface viscosity at the surface layers), as has been done in different works (Vorobieff et al. 2001; Prasad and Weeks 2009). The elastic Mach number $M_e = U/v_e$ introduces the elastic behaviour of the film and it compares the characteristic velocity of the film with the elastic wave velocity $v_e = \sqrt{\frac{E}{\rho H}}$ where E is the effective elasticity coefficient and ρ is the fluid mass density. Finally, the parameter $\Upsilon = \frac{UHc}{J_{ad}L}$ compares the advective flow of surfactant through the film thickness and the adsorption flux J_{ad} along the characteristic length of the flow. Depending on the relative values of these parameters, different scenarios can occur. Particularly, it is interesting the case when $\frac{d(\Gamma A)}{dt} \simeq 0$ (being A the film surface). In this situation, E is the Marangoni elasticity and for sub-critical regimes when $M_e < 1$ the 3D soap flow may found an analogous 2D flow.

The classical theoretical analysis of soap film dynamics is performed looking for a solution with an expansion

of all variables in terms of a small parameter $\epsilon = \frac{H}{L}$ where H is the undisturbed film thickness and L is the characteristic length of the flow. With this approach (Auliel et al. 2015) we have found that in the range of the subcritical regimes when $M_e = 0_{(10^{-1})}$, a typical situation in vertical soap film experiments, at leading order the soap film dynamics agrees with a 2D divergence free flow with packets of non-uniform density. We could also determine that in soap films a source of vorticity may appear, absent in the analogous 2D flows, that is related to the non-alignment of thickness gradient with the gradient of concentration of surfactant at the surface. In the inviscid limit ($Re \longrightarrow \infty$), this is expressed by

$$\frac{D_0\boldsymbol{\varpi}}{Dt} = \left(\frac{1}{ZM_e}\right)^2 \boldsymbol{\nabla_0} Z \times \boldsymbol{\nabla_0}\Gamma_0, \tag{3}$$

being $Z = 1 + \frac{\eta}{H}$ (see Fig. 1) and ϖ the 2D vorticity. This "baroclinic" source of vorticity particularly may play an important role in proximity of the wall of objects inserted in the flow. The meniscus there created is expected to produce differences between soap film dynamics from the equivalent 2D flow with the same object.

Where this effect is not important, the surface soap concentration can be related to the role of classical pressure p and the equivalent density is ZM_e^2. Both magnitudes are linked through the following equation

$$\nabla_0^2\Gamma_0 \sim \frac{M_e^2}{ReZ^2} W_2. \tag{4}$$

Here $\Gamma_0 = \frac{\gamma_0}{\gamma_m}$ is the non-dimensional surfactant concentration at the interface (γ_m is the mean surface concentration), and $W_2 = \frac{D\eta_2}{Dt}$. The sub-index indicates the order of the expansion. The sign of the right hand side of this equation depends on the sign of the normal velocity that is found to be non null at the second order of the expansion.

In divergence free flows, the general pressure Poisson's equation reads:

$$\nabla^2 p = -\rho\boldsymbol{\nabla}\cdot(\boldsymbol{u}\cdot\boldsymbol{\nabla}\boldsymbol{u}) - \boldsymbol{\nabla}\rho\cdot(\boldsymbol{u}\cdot\boldsymbol{\nabla}\boldsymbol{u}). \tag{5}$$

When mass density is uniform the source term of Poisson's equation (right hand side of expression 5) reduces to

$$-\rho\boldsymbol{\nabla}\cdot(\boldsymbol{u}\cdot\boldsymbol{\nabla}\boldsymbol{u}) = \rho\Lambda^2. \tag{6}$$

The parameter Λ is defined as $\Lambda^2 = \frac{1}{2}(\varpi^2 - s^2)$ with (ϖ^2) the squared vorticity and the squared rate of strain $(s^2 = \left[\frac{\partial u}{\partial x} - \frac{\partial v}{\partial y}\right]^2 + \left[\frac{\partial u}{\partial y} + \frac{\partial v}{\partial x}\right]^2)$. This parameter agrees with the value of the second invariant of the velocity gradient tensor of the 2D flow. In 2D incompressible flows, the value of the invariant is customarily used as a vortex identification criterion (Q or Okubo–Weiss criterion) (Weiss 1991). Such criterion may be established on the basis of dynamical arguments involving a comparison between the squared vorticity (ϖ^2) and the squared rate of strain (s^2) or considering local topological aspects of velocity fields (Larchevêque 1993; Rivera and Wu 2000).

When ZM_e^2 is low enough, a second expansion can be proposed in terms of this variable, and at leading order the soap flow behaves as a uniform density flow and an analogy between Eqs. 4 and 5 is found. The Laplacian in these equations is positive in the core of low pressure regions (low—Γ_0 regions) and becomes negative in the core of high pressure regions (high—Γ_0 regions) (Larchevêque 1993). Considering Eq. 6 one can see that low pressure regions can be associated to regions that tend to form humps and high pressure regions to those that tend to form depressions in the film.

It is appropriate to mention that the sign of the invariant enables in general the partitioning of regions of the flow: those with positive values of the invariant are usually named elliptic domains, while the regions with negative values are named hyperbolic domains. It is expected that regions with the largest thickness variation correspond to regions of the flow with presence of strong centers (high elliptic regions) or saddles (high hyperbolic regions). It is of interest to signal that in turbulent 2D flows a universal asymmetric PDF of the distribution of the value of the invariant has been stated (Rivera et al. 2001) with its peak at the zero value and biased towards the positive values. Histograms of thickness of soap films with grid turbulence have shown the same kind of distribution (Greffier et al. 2002).

2.3 Soap film velocimetry based on images

Techniques of image velocimetry based on correlation-methods, like PIV, are well established in the fluid mechanics community. Jonassen et al. (2006) have extended the used of traditional PIV algorithms (with particle tracers) to Schlieren images of 3D flows (around Helium jet and a compressible turbulent boundary layer) and show results in which they were able to derive the time averaged flow fields. These authors considered as photometric pattern the mass density spatial variations associated to the fine scale turbulent eddies and assumed that the brightness associated to these patterns was kept constant between two successive images. They proposed rules to tune the contrast of the Schlieren images for velocimetry purposes considering the criteria established when photometric patterns are the conventional seeding particles.

Particle Image Velocimetry analysis with Schlieren images of 2D turbulent soap film flows can be proposed considering as photometric patterns the gradients of the film thickness and assuming the non-evolution of its components on the interval of time between two successive images.

However, there are some intrinsic restraints in the use of Particle Image Velocimetry techniques that may discourage the use of this velocimetry estimator. On one hand, the use of interrogation windows, inside which velocity is assumed to be uniform, may produce a filtering of the fine scales details of the flow and alter turbulent spectra. On the other hand, it is well known that methods based on correlation may lose accuracy when considering small interrogation windows, or regions with large velocity gradients or scalar images (Heitz 2010). These situations may appear when analysing turbulent soap film flows with Schlieren images and the so-called global methods can be considered as a suitable alternative to minimize these problems. One of the most accurate techniques of this group of methods are those derived from the Horn and Schunck optical flow estimator (Berthold 1981; Black and Anandan 1996; Mémin and Pérez 2002; Ruhnau et al. 2005). Such kind of estimators are formalized as minimizers of an energy function composed of a data term and a regularization term. The first one describes a consistency assumption of the luminance function along a point trajectory. The regularization term captures an a priori on the displacement field. A standard first-order spatial smoothness is usually considered.

There have been efforts to develop dense motion algorithms specially dedicated to sequences of Schlieren images (Wang et al. 2015). Some of the authors of the present manuscript have previously given contributions in this field considering as assumption isotropy of the density gradients in the plane of motion (Sosa et al. 2006). The use of this kind of approach is relevant when the time between two frames is large enough and brightness constancy of fluid particles between two images cannot be assured. Even the schemes developed could be generalised to be used with Schlieren image of soap film flows, we prefer to simplify the analysis by restricting the conditions of image acquisition and assume that the simple brightness constancy can be accepted. Within this framework and provided the displacement field between images is small and smooth, dense fields are possible to be derived considering simple global approach. The one we consider has been proposed by Quenot and details of its implementation are described in the section dedicated to the analysis of results issued from the use of this optical flow method. More sophisticated approaches can be found, for instance, in Dérian et al. (2013).

3 Experimental setup

3.1 Soap film tunnel setup

The experiments were carried out in a vertical flowing soap film (see Fig 2). The soap film tunnel consists of a pair of nylon guide wires (diameter 520 µm) splaying from the

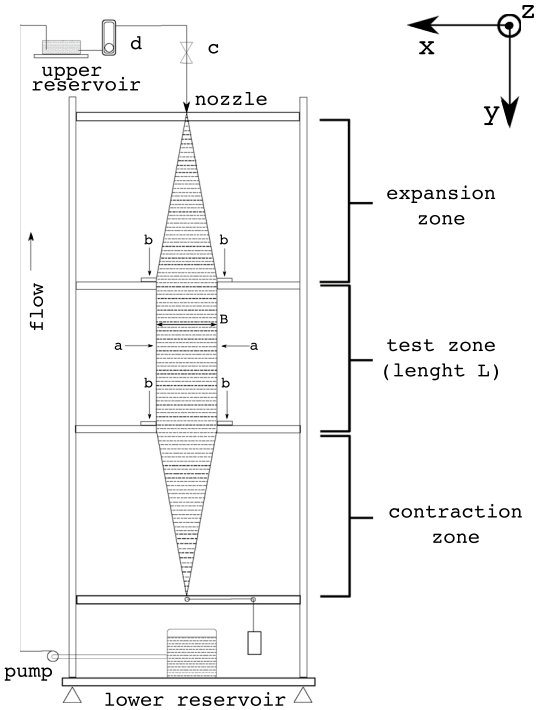

Fig. 2 Sketch of the vertical flowing soap film. **a** Nylon threads, **b** fishing lines, **c** valve and **d** flowmeter

nozzle. Four thinner nylon fishing lines (diameter 120 µm) were attached to the guide wires to hold them apart allowing an adjustable tunnel breath (B). As the fluid solution is ejected from the nozzle it stretches between the guide wires as it is accelerated by gravity in the expansion section of the channel.

The test section is the region where the guide wires are parallel and there the film reaches an almost constant velocity (V) due to the balance between gravitational and air drag forces (Rutgers 1998). This section has a maximum breath (B_{mx}) of 180 mm and a length (L) of 590 mm. The tunnel enables flow velocities (V), ranging between 0.8 and 5.0 m/s, that can be adjusted with a metering valve (c) that controls the injection rate at the top of the tunnel.

More downstream, the tunnel has a contraction section which is designed to collect the fluid at the bottom of the tunnel into a reservoir.

In our study, the liquid flowing in the tunnel was a solution composed of with a mixture of 2%, in volume, of liquid commercial detergent in fresh water.

A first group of experiments was undertaken introducing a smooth cylinder on the flowing film to produce a wake flow. The cylinder was an aluminium rod with a diameter (D) of 10 mm. The breath of the test section was fixed at 80 mm resulting in a flow blockage ($b = D/B$ 100) of 12.5%.

The flow rate (Q), measured by a flowmeter (d), for these experiments was fixed at 40 ml/min (±2 ml/min). Tracking

some small bubbles, or particles, occasionally present in the flowing soap film, we have roughly measured the typical flow velocities for this experiment around $V \simeq 2.2$ m/s.

A second set of experiments considered a grid turbulent flow (Auliel 2016). The vertical soap film channel for this kind of experiment was set to a width of 75 mm. The grid used to generate turbulence was a comb composed by a single row of small cylinders aligned along 61 mm. The separation between teeth was of 5.1 mm and the diameter of each tooth of 3.1 mm. The flow rate, measured by a flowmeter, was set to 80 ml/min and associated mean velocity of 3.8 m/s (see Fig. 3).

3.2 Optical arrangement

In this study, we have employed a "Z-type" or Herschelian arrangement composed by two oppositely tilted on-axis parabolic concave mirrors.

We have used two mirrors with a diameter of 300 mm and focal length of 1.6 m. The distance between mirrors was set to 3.8 m. The illumination was produced with a led lamp of 100 W whose intensity could be adjusted with the power source to which it was connected. A condenser lens and a rectangular slit was used to achieve an almost point source of light. Our arrangement included a pair of separated vertical and horizontal knife edges positioned at the tangential and sagittal foci. These blades were used to obstruct the deviated light rays and to improve the contrast of the otherwise shadowgraph image that would be formed at the CCD of the video camera. The astigmatism of the z-type arrangement we used frustrated the use of any device (circular or L-shaped) that attempted to mask the light beam in a single x–y plane. The setup used allowed us to produce either horizontal, or vertical or simultaneous cut-offs in both directions. Hence, horizontal, vertical or both components of the gradient of thickness can be detected giving the opportunity to achieve finer adjustment of the contrast to the experimental conditions of the flow.

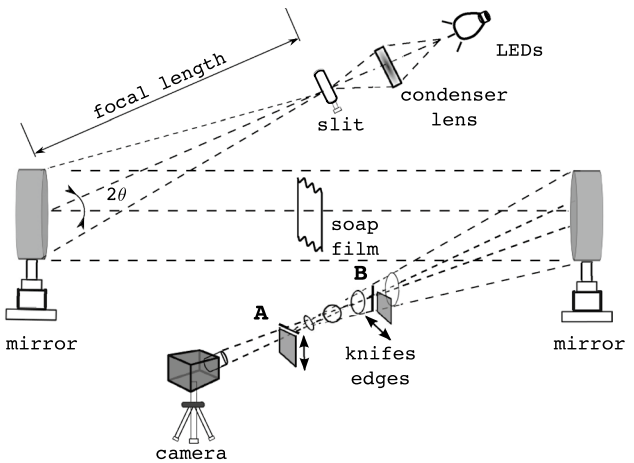

Fig. 3 *Herschellian* system considered. **a** Sagittal focal plane. **b** Tangential focal plane

For image acquisition, we used a monochromatic high speed video camera (3000 frames/s with a resolution of 512×512 pixels^2). The typical exposure time was 200 μs and the lens used was a Fuji of 16–160 mm, $f = 1{:}2.5$, zoom in 140/160 mm and infinite focus.

To enable image comparisons we also mounted another optical setup for studies with the interferometric technique. The angle of incidence of the light with the normal of the undisturbed film surface α_i was set close to 13°. To record the images, a camera (the same of the Schlieren set-up) was disposed symmetrically to the xy soap film plane and at a distance of 700 mm from film surface. The typical exposure time was 200 μs and the lens used was a 75 mm, $f = 1{:}1,8$ with infinite focus. Illumination was produced with a set of 12 rows $\times 24$ columns of LEDS of 1 W disposed in a square section of 35×35 mm^2. To decrease light intensity and achieve a more uniform illumination, sheets of tracing paper were used as a diffuser. A number of 256 of these LEDS emitted with a wavelength between 620 and 660 $\dot{A}$ (red-violet) and 32 of them between 450 and 470 $\dot{A}$ (blue). In these conditions, the thickness variation between two consecutive maxima of the image was $\Delta h = 180$ nm.

4 Results and discussion

4.1 Analysis of images

With our experimental conditions (film thickness in the order of μm) the interferometric technique appears as an adequate technique to visualize film thickness variation. This technique has associated parallax errors that appear as a consequence of the inclined vision of the region of interest. This error is minimized by reducing the angle formed by the incident light and the camera. However, a compromise is present as the minimization of this angle reduces the range of measurement of the thickness gradients. A drawback of the technique is that the adjustment of the quality of images is done for each experiment changing the positions of the source and camera.

Visualizations of soap film flows with the Schlieren technique enable the detection of thickness gradients and has the advantage of easily improving the image contrast by adjusting the light intensity and the amount of light that the knife-edge cuts off. This tuning determines the range of deflected angles accepted. As drawback, Schlieren requires high quality mirrors, as those with short focal length have associated astigmatism errors, and a careful optical alignment.

It is of interest to try to link the intensity of the images produced by visualizations of the soap film with magnitudes observed in equivalent 2D flows. Considering the theoretical aspects described in Sect. 2, for experiments performed in the sub-critical range, the dynamics of the film thickness can be associated to the dynamics of the extrema of the analogous pressure field and one can in general associate regions of gradients of the thickness with regions of high or low pressure. Relevant information may be extracted from direct observation of images obtained with the interferometry technique and monochromatic light. The lines of constant intensity can be associated to lines of constant thickness and concentrations of this contour-lines indicate gradients of thickness. Furthermore, when the flow can be considered as an almost constant density flow, concentration of quite axis-symmetric iso-lines of interferometric images can be associated to strong centers or strong vortex cores (Daniel and Rutgers 2002). Depending on the cut off of light produced by the knife edges the contour lines of Schlieren images are iso-lines of single components of the gradient of thickness or the addition of both. Therefore, they enable an easy direct identification of saddles or centers (low or high pressure regions) by direct observations of intensities in a single snapshot.

4.1.1 Wake flow images

We show images of this kind of experiment because its cyclic behaviour enables an easy comparison of interferometry and Schlieren technique. Images obtained not simultaneously but corresponding almost to the same phase of the cycle can be confronted. The results we show in these figures correspond to flows in which the measured non-dimensional frequency (Strouhal number) $\mathrm{St}_{vs} = f_{vs}D/U_\infty$ was ~ 0.19 (where f_{vs} the vortex shedding frequency). The Reynolds number $Re = U_\infty D/\nu$ was close to a value of 4000 with an effective kinematic viscosity of the soap film (ν) estimated close to 5.510^{-6} m^2/s. This value was obtained measuring frequencies of the wakes generated by pinching the film with cylinders of different diameters and using the Strouhal vs Reynolds number curve of Roushan et al. Roushan and Wu (2005). Images were captured at 2500 frames/s with an exposure time of 250 µs.

In left Figs. 4 and 5 the interferometric images show iso-lines of intensity that seem quite in correspondence with the pressure field on the front part of the flow around a cylinder. With the Schlieren system the image upstream the object is quite smooth. Downstream, the presence of the obstacle generates vorticity that is detached from the wall. The "baroclinic" source of vorticity may take importance at wall proximities, and in the near wake the vorticity field of soap film can not be directly associated to the pressure field of a quasi analogous 2D flow. Particularly, it is possible

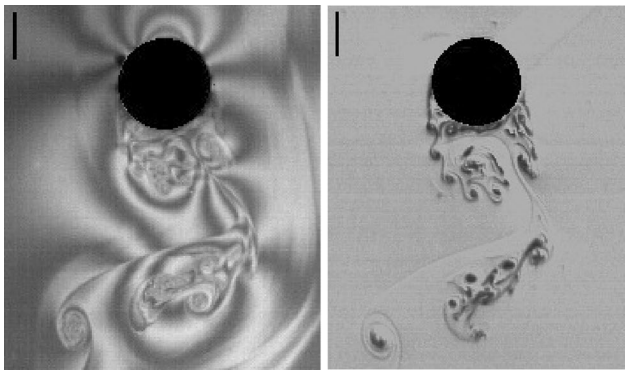

Fig. 4 Images of the wake flow. (*left*) Interferometry technique, (*right*) Schlieren technique. Both images are not simultaneous. The segment on the *left* is a scale that represents 0.5 cm

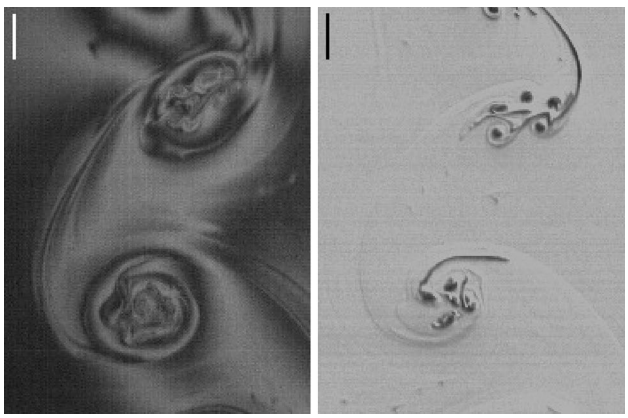

Fig. 5 Images of the wake flow four diameters downstream the cylinder (*left*) Interferometry technique, (*right*) Schlieren technique. Both images are not simultaneous. The segment on the *left* is a scale that represents 0.5 cm

to observe fine structures inside the core of vortex that do not correspond with pressure fields of similar wake flows. The Schlieren images enable a quite direct identification of vortex centers. These images show sharp structures downstream the cylinder that look like transition eddies along the free shear layer spiralling and forming a larger eddy. These structures are reminiscent to eddies configurations that have been depicted for cylinder wake flows long time ago (Zdravkovich 1977, 1985; Courregelongue 1929). We can explain this property of Schlieren images, considering that regions with high values of the thickness gradients correspond to regions of the flow with the presence of strong centers or saddles. Thus, as contrast of Schlieren images is proportional to the components of the thickness gradient (meanwhile for the interferometric technique this does not hold) the cores of vortex are more easily identified with

Schlieren than with interferometric technique, as this wake flow images illustrate.

4.2 Quantitative analysis

Images with interferometric technique and Schlieren technique of grid turbulence are shown on Fig. 6, left and right, respectively. These images are taken 10 cm downstream the grid position. These kind of images are attractive because of their texture and the possibility they open to obtain dense vector fields in the region of interest without the use of external tracers.

On Fig. 7, left and right, respectively, we show histograms of the intensity of the images for interferometric and Schlieren techniques. The histogram for Schlieren images exhibits an asymmetric distribution that looks like the ones observed for the thickness variation histograms found by other researchers (Greffier et al. 2002). Considering the theoretical aspects described in Sect. 2 a link between PDF of Schlieren intensity and PDF of the invariant Λ can be proposed. As we will show in a next section both exhibit the same asymmetric shape.

4.3 Velocimetry from the scalar images

In this section, we discuss aspects of the possible tracking of the visualized photometric patterns. In situations where thickness behaves as material particles advected by the flow the use of Particle Image Velocimetry or Optical Flow techniques are of interest because the spot of thickness can be used as a tracer. As, at first order, the soap film dynamics is divergence free and thickness variation along time is expected to be small. The brightness of fluid particles in interferometric images remains almost constant with time and enables the use of theses images for velocimetry purposes.

The use of Schlieren images with this technique is not so straightforward because brightness constancy assumption requires the gradient of images to be almost constant along

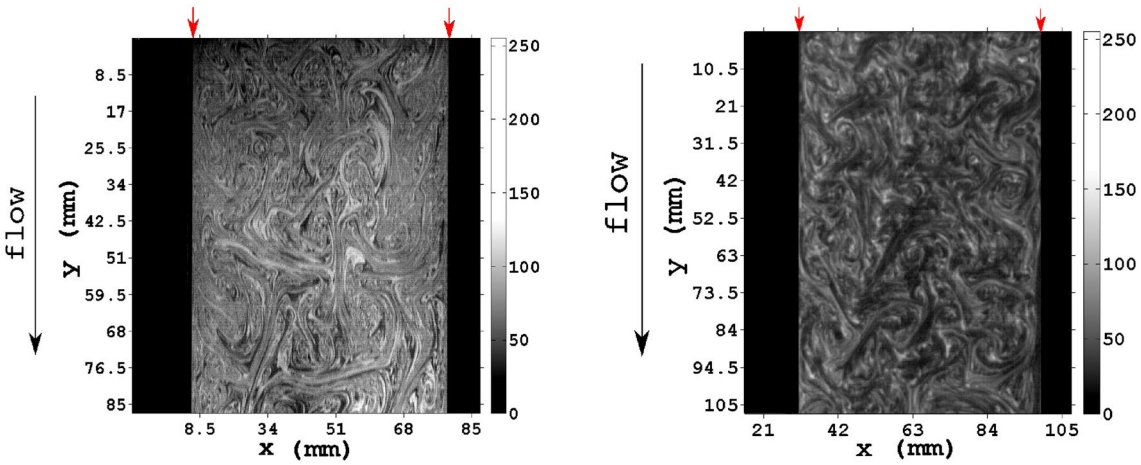

Fig. 6 Images of the grid turbulence. *Left* Interferometry technique, *right* Schlieren technique using vertical and horizontal knives. Both images are not simultaneous. The *arrows* indicate the location of the guide wires

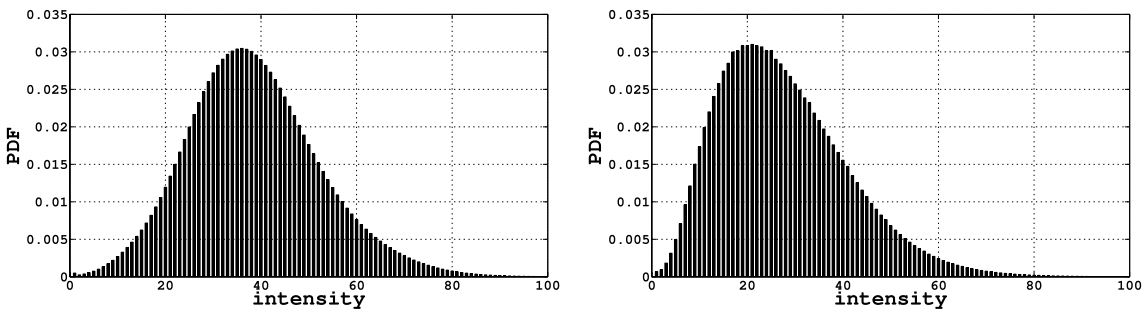

Fig. 7 Histograms of intensity (*left*) interferometry technique, *right* Schlieren technique using vertical and horizontal knives

time. Let us analyse the variations of the thickness gradient when the thickness of the film is preserved. We can write

$$\frac{d\nabla\eta}{\mathrm{d}t} = -\nabla\boldsymbol{u}\cdot\nabla\eta. \tag{7}$$

When the thickness gradient varies more rapidly than the velocity gradient, the eigensolutions of the above equations are $\| \nabla\eta \| \propto e^{\Lambda t}$, where again Λ^2 is the eigenvalue of the velocity gradient. In regions of vorticity dominance, the thickness gradient is locally preserved and vortex particles will tend to keep their intensity between two frames, provided that the diffusive time scale of the eddies is much longer than the time separation of the images pair. In regions where Λ^2 is positive, the $\| \nabla\eta \|$ evolves in time. Nevertheless, the changes in intensity associated with the stretching can be minimized reducing the time between two consecutive exposures.

As explained in different articles, the PIV technique may not be fully adequate to post-process scalar images and derive dense velocity fields. We show results obtained with this technique as a suitable framework for the analysis of the dense motion estimator described in next section. The PIV records have been analysed with a commercial software using a cross-correlation technique implemented with a fast Fourier transform algorithm in a multi-grid process. In our case, we chose a final square windows 12×12 pixels^2 with a 50% overlapping between windows. In the multipass option, the initial window size is halved in each step until final size is reached. Post-processing images with this kind of technique enabled us to obtain 1 vector each 1.6 mm^2 and 1.1 mm^2 for Schlieren and interferometry tests, respectively.

To obtain dense vector field we have considered an optical flow technique whose algorithm is based on a transformation that relates the first image to the second by minimizing the Minkowski distance between them (Quénot 1992, 1996, 1998). The following two assumptions are expected to hold for the algorithm to work properly: the gray level (intensity) of two displaced particles are conserved and the displacement is small compared to the image size. It is expected that these hypotheses will be verified for short time between two successive exposures. Prior to the application of the algorithm, the raw image of the flow is preprocessed with a standard technique of this dense motion estimator that combines a high-pass filter and a local intensity mean and standard deviation normalization. The use of this technique with our experimental arrangement enabled us to obtain 1 vector each 0.04 mm^2 and 0.02 mm^2 for Schlieren and interferometry tests, respectively.

4.3.1 Velocimetry results

We analyse and compare here results using the techniques we have described in the preceding section (PIV and optic flow). The goal is to try to validate the techniques and compare the results of velocimetry based on interferometry and Schlieren images. To undertake this task, we rely on the comparison of our results with those of other researchers concerning statistical properties of turbulence confined to two spatial dimensions.

For this comparison we consider the temporal Fourier spectra, the probability density functions of centers and saddles and structure functions. Even if a more exhaustive analysis could be performed, we limit our analysis to these three properties just to illustrate some of the salient features and validate the methodology we propose.

Results concerning the first group can be observed on Figs. 8 and 9. To analyse the quality of the methodology, a comparison of the inertial ranges can be undertaken. Let us use the Taylor frozen turbulence assumption considering that previous works indicate that this hypothesis seems to work well in soap film (Belmonte et al. 2000). In this case, we can assume that the eddies are swept by the mean flow and traverse the observation region without important changes in their structure. A conversion of wavenumbers to the frequencies can be proposed, giving as a result that the velocity power spectra scales with the wavenumber in the same way it scales with frequency. The scaling of the velocity power spectra or, equivalently, the energy density spectrum, have to be consistent with predictions of the

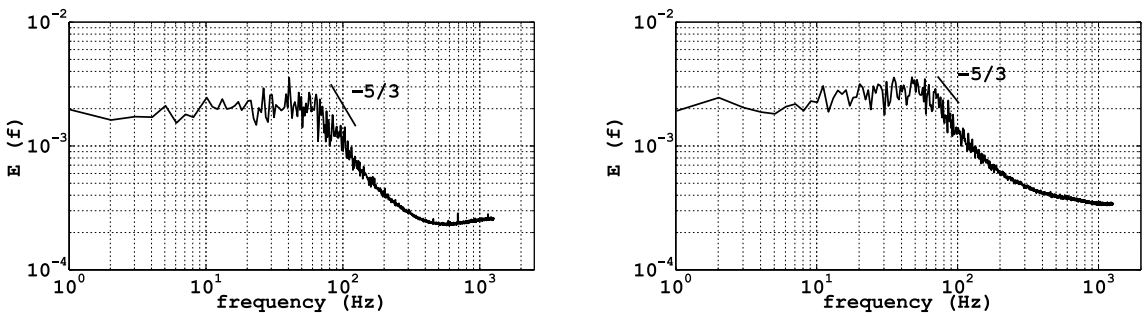

Fig. 8 Turbulence spectra using PIV—*left* interferometry technique, *right* Schlieren technique using vertical and horizontal knives

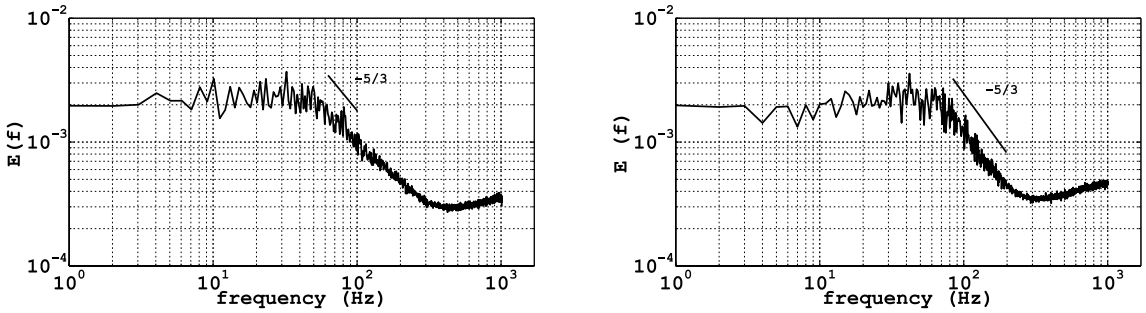

Fig. 9 Turbulence spectra using optical flow—*left* interferometry technique, *right* Schlieren technique using vertical and horizontal knives

phenomenological theories of 2D turbulence. These theories predict a scaling law for these spectra with an exponent $-5/3$ for the inverse cascade range and of -3 for the direct cascade range. It is expected that the analysed turbulent flow exhibits features of decaying 2D turbulence with ranges of the direct cascade and inverse cascade depending on the distance to the grid (Rutgers 1998).

The inspection of the figures indicate that the results are observed when using Schlieren images combined with optical flow technique are in better agreement with the theory of 2D turbulence. The slope of $-5/3$ is unambiguously retrieved in a larger range compared with the other cases in which a smaller exponent tends to prevail. This indicates that the tracking of Schlieren photometric patterns enable a finer resolution than the ones of Interferometry technique. The direct cascade range, however, cannot be detected with clarity in any of these graphs, probably because the resolution at these small scales was not high enough.

This result can be complemented with other ones to qualify the methodology. Let us focus on a second test performed considering the structure functions. The structure function of order n, $S_n(r)$, defined as

$$S_n(r) = \langle |\delta \mathbf{u}(\mathbf{r})|^n \rangle \equiv \langle |\mathbf{u}(\mathbf{x}+\mathbf{r}) - \mathbf{u}(\mathbf{x})|^n \rangle, \tag{8}$$

scales in general as a power law of the distance r, with an exponent ζ_n. For the analysis of the inertial range of structure functions, the hypothesis of extended self-similarity (ESS) is usually accepted (Benzi et al. 1993). When the flow is self-similar, ζ_n equals n / 3 (Frisch and Kolmogorov 1996), and in the absence of intermittency of turbulence, ζ_n has a monotonic growth relationship with n (Kraichnan 1967; Boffetta et al. 2002).

In Fig. 10, the structure functions 1, 2 and 3 are shown for optical flow velocity fields obtained from the interferometric and Schlieren images, respectively. Axes are in logarithmic scales and the solid lines correspond to the slopes of 1/3, 2/3 and 1. The graphs show that the length of inertial ranges obtained with interferometry appear shorter than those obtained with Schlieren. The values of the slope in these regions (estimated by the Least Squares Fitting) are within the values expected from the literature (Kraichnan 1967), with errors less than 10%.

To check the performance of the methodologies concerning intermittency phenomena, we constructed Fig. 11, which shows the slopes obtained for each structure functions in the inertial range against the value of the order n. In these figures, we observe a monotonical growth of the slope with the order of the function structure and a good fitting of data with a linear function. Both, the Schlieren

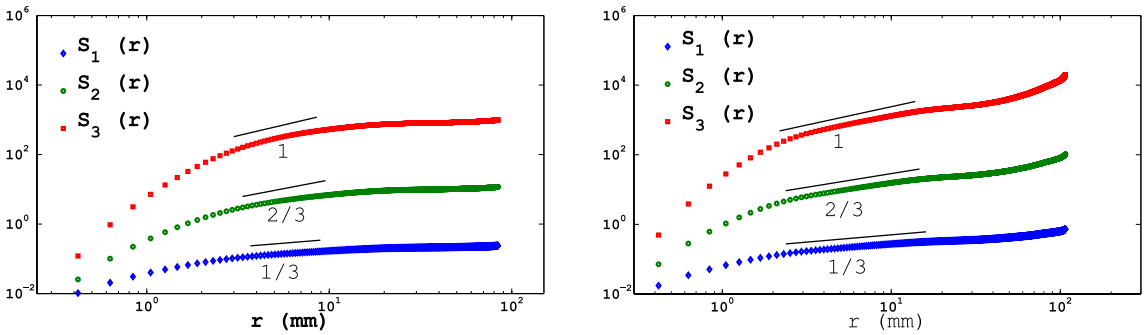

Fig. 10 Structure functions of order 1, 2 and 3 obtained from images with interferometry technique (*left*) and Schlieren technique (*right*)with optical flow technique. Figure axes are logarithmic scales. The *solid lines* correspond to the slopes of 1/3, 2/3 and 1

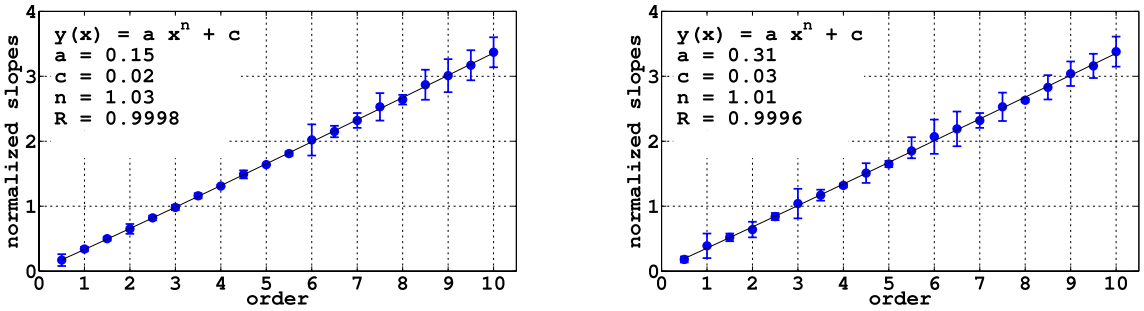

Fig. 11 Relation between the slopes of the functions order structure from 0.5 to 10, in intervals of 0.5, normalized by the value of the slope of S_3 vs. order for interferometry images (*left*) and Schlieren images (*right*)

and interferometry results, show a good agreement with the results reported by other researchers (Jun and Wu 2005; Paret and Tabeling 1998). The absence of intermittency effects in the flow is verified with these data, as up to the order 10 no significant deviations from the linear fitting occur.

Finally, we propose another tool of analysis based on the statistics of saddles and centers. This statistic property seems to be universal, independent of turbulent intensity and the means of turbulence generation (Daniel and Rutgers 2002). Therefore, it gives an appropriate strategy to evaluate the velocimetry results.

To undertake this analysis, the parameter Λ is here derived from velocity fields obtained with optic flow technique. Previous results have shown that the PDF of the invariant strongly deviates from a Gaussian behaviour, exhibiting for large values of $|\Lambda|$ prominent exponential tails. Furthermore, the $P(\Lambda)$ is nonanalytical at $\Lambda = 0$ and decays more slowly for positive Λ or equivalently for centers. This kind of results has been verified experimentally with a decaying and an electromagnetically forced 2D turbulent flow. The authors proposed this law to be universal in 2D turbulence, with independence of turbulence intensity and the means of turbulent generation (Rivera et al. 2001). Therefore, they should be observed in our experiments. To facilitate comparison, we undertake the same normalization as these authors did (with the root mean square values of the invariant). We can observe on Fig. 12 that in both cases we found asymmetric curves that lie almost in the same range observed by these researchers. In both cases, the larger propensity of the flow to form strong vortex centers relative to saddle points of comparable magnitude is retrieved. We can also observe that the PDF is non-analytic towards the origin in both cases. The shapes of the curves obtained with the Schlieren technique are, however, much more in agreement with observations of other works especially in the positive tails of the curve where the estimations issued from interferometric data seem less accurate (Daniel and Rutgers 2002).

5 Conclusions

We have introduced the use of Schlieren technique as a new method to visualize the flow dynamics of soap films. This technique, as interferometry also does, relies on the perturbations of the thickness of the film produced by the flow. The images obtained with both techniques are, however, different. The lines of constant intensity of interferometric images can be associated to lines of constant

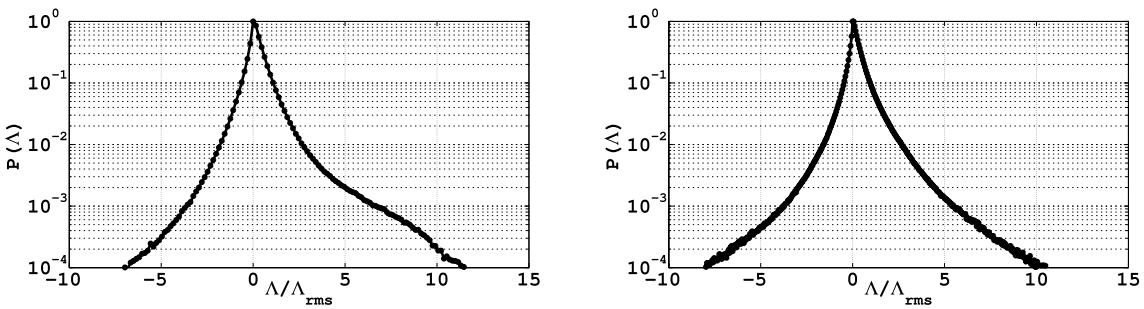

Fig. 12 PDF of Λ/Λ_{rms}, *left* interferometry technique, *right* Schlieren technique using vertical and horizontal knives

thickness meanwhile for Schlieren images correspond to the components of the gradient of thickness.

Regions where vorticity dominates can be clearly identified with the Schlieren technique by simple visual inspection of the images as in these regions gradients of film thickness are significant. This has been illustrated with images of wake flows that we have shown as example in our work. The analysis of grid turbulent flows show that the PDF function of intensity of interferometric images is Gaussian while with Schlieren technique is asymmetric. This bias is in agreement with results obtained by other researchers that have found a propensity of these flows to create humps in the film rather than depressions.

When the time elapsed between the acquisition of a pair of successive images is short enough constancy of brightness of the patterns of the scalar image can be assumed. An attractive aspect of these images is that the photometric patterns are produced without the external seeding of the flow. Therefore, velocimetry methods based on these images can give information of the velocity field without the limitations associated with the use of tracer particles. The velocimetry techniques can provide results of flow fields in regions where thickness gradients are present and advected by the flow.

We have tested the use of a simple dense motion estimator to obtain spectra of a grid turbulent flow. Compared to interferometric results the Schlieren images were able to detect a larger inertial range with an exponent close to the theoretical one of $-5/3$. The analysis of structure functions corroborates that inertial ranges found by Schlieren technique are larger than those retrieved by interferometry and also show the absence of intermittency phenomena for the analysed flow.

We have finally considered the statistics of the second invariant of the velocity gradient tensor and studied the probability density functions of centers and saddles. Both techniques retrieve the salient features of these PDF curves: an asymmetry towards the regions associated to centers and a non-analyticity of the distribution function at the origin. Again, the statistics of velocity fields obtained with Schlieren images are found to agree with the results obtained by other researchers in a larger range than the one observed when using interferometric images. The asymmetries found in the PDF of intensities of Schlieren images and of the second invariant are coupled and can be explained considering the equations that describes this soap film dynamics for the sub-critical range. In summary, the methodology we propose opens new possibilities to experimental studies of bidimensional turbulent flow. We hope future works will help to improve the motion estimators to be used and therefore increase the understanding of these flows.

References

Amarouchene Y, Kellay H (2004) Batchelor scaling in fast-flowing soap films. Phys Rev Lett 93:214504

Auliel MI, Castro F, Sosa R, Artana G (2015) Gravity-driven soap film dynamics in subcritical regimes. Phys Rev E 92:043009

Auliel MI (2016) Estudio de leyes de escala turbulentas y su vínculo con propiedades macroscópicas de flujos. PhD thesis, Departamento de Ingeniería, UBA, Ciudad Autónoma de Buenos Aires, Argentina

Belmonte A, Martin B, Goldburg WI (2000) Experimental study of taylors hypothesis in a turbulent soap film. Phys Fluids 12(4):835–845

Benzi R, Ciliberto S, Tripiccione R, Baudet C, Massaioli F, Succi S (1993) Extended self-similarity in turbulent flows. Phys Rev E 48:R29–R32

Berthold K, Horn P, Schunck BG (1981) Determining optical flow. Artif Intell 17:185–203

Black MJ, Anandan P (1996) The robust estimation of multiple motions: parametric and piecewise-smooth flow fields. Comput Vis Image Underst 63(1):75–104

Boffetta G, Celani A, Musacchio S, Vergassola M (2002) Intermittency in two-dimensional ekman-navier-stokes turbulence. Phys Rev E 66(2):026304

Cabaleiro JM, Aider JL, Artana G, Wesfreid JE (2013) Single camera time-resolved 3d tomographic reconstruction of a pulsed gas jet. J Vis 16(4):263–274

Chomaz JM (2001) The dynamics of a viscous soap film with soluble surfactant. J Fluid Mech 442:387–409

Couder Y, Chomaz JM, Rabaud M (1989) On the hydrodynamics of soap films. Phys D Nonlinear Phenom 37(1):384–405

Courregelongue J (1929) Sur lexistence de deux familles de tourbillonsa larriére des solides immergés. CR Acad Sci Paris 189:972–974

Daniel WB, Rutgers MA (2002) Topology of two-dimensional turbulence. Phys Rev Lett 89(13):134502

Dérian P, Héas P, Herzet C, Mémin E (2013) Wavelets and optical flow motion estimation. Numer Math Theory Methods Appl 6(01):116–137

Frisch U, Kolmogorov AN (1996) Turbulence: the legacy of A. N. Kolmogorov. Cambridge University Press

Goldstein R (1996) Fluid mechanics measurements. CRC Press

Greffier O, Amarouchene Y, Kellay H (2002) Thickness fluctuations in turbulent soap films. Phys Rev Lett 88:194101

Hargather MJ, Lawson MJ, Settles GS, Weinstein LM (2011) Seedless velocimetry measurements by schlieren image velocimetry. AIAA J 49(3):611–620

Heitz D, Mémin E, Schnörr C (2010) Variational fluid flow measurements from image sequences: synopsis and perspectives. Exp Fluids 48(3):369–393

Huang MJ, Wen CY, Lee IC, Tsai CH (2004) Air-damping effects on developing velocity profiles in flowing soap films. Phys Fluids 16(11):3975–3982

Isenberg C (1992) The science of soap films and soap bubbles. General Publishing Company, dover edition edition, Don Mills

Jonassen DR, Settles GS, Tronosky MD (2006) Schlieren piv for turbulent flows. Opt Lasers Eng 44(3):190–207

Jun Y, Wu XL (2005) Large-scale intermittency in two-dimensional driven turbulence. Phys Rev E 72:035302

Kellay H, Wu XL, Goldburg WI (1998) Vorticity measurements in turbulent soap films. Phys Rev Lett 80:277–280

Kellay H, Wu XL, Goldburg WI (1995) Experiments with turbulent soap films. Phys. Rev. Lett. 74:3975–3978 1995. s

Kraichnan RH (1967) Inertial ranges in 2 dimensional turbulence. Phys Fluids 10:1417

Larchevêque M (1993) Pressure field, vorticity field, and coherent structures in two-dimensional incompressible turbulent flows. Theor Comput Fluid Dynam 5(4):215–222

Mémin E, Pérez P (2002) Hierarchical estimation and segmentation of dense motion fields. Int J Comput Vis 46(2):129–155

Paret J, Tabeling P (1998) Intermittency in the two-dimensional inverse cascade of energy: experimental observations. Phys Fluids (1994-present) 0(12):3126–3136

Prasad V, Weeks ER (2009) Flow fields in soap films: relating viscosity and film thickness. Phys Rev E 80(2):026309

Quénot GM (1992) Theorthogonal algorithm'for optical flow detection using dynamic programming. In: Acoustics, speech, and signal processing, 1992. ICASSP-92., 1992 IEEE International Conference on, vol 3, pp 249–252. IEEE

Quénot GM (1996) Computation of optical flow using dynamic programming. In: IAPR Workshop on Machine Vision Applications, pp 249–252

Quénot GM, Pakleza J, Kowalewski TA (1998) Particle image velocimetry with optical flow. Exp Fluids 25(3):177–189

Rivera M, Vorobieff P, Ecke RE (1998) Turbulence in flowing soap films: velocity, vorticity, and thickness fields. Phys Rev Lett 81(7):1417

Rivera M, Belmonte A, Goldburg WI, Wu XL, Kellay H (1998) Optical fiber velocimetry: a technique for measuring velocity in two-dimensional flows. Revi Sci Instr 69(9):3215–3222

Rivera M, Wu XL, Yeung C (2001) Universal distribution of centers and saddles in two-dimensional turbulence. Phys Rev Lett 87:044501

Rivera M, Aluie H, Ecke RE (2014) The direct enstrophy cascade of two-dimensional soap film flows. Phys Fluids (1994–present) 26(5):055105

Rivera M, Wu XL (2000) External dissipation in driven two-dimensional turbulence. Phys Rev Lett 85:976–979

Rivera M, Wu XL (2002) Homogeneity and the inertial range in driven two-dimensional turbulence. Phys Fluids 14(9):3098–3108

Roushan P, Wu XL (2005) Structure-based interpretation of the strouhal-reynolds number relationship. Phys Rev Lett 94:054504

Ruhnau P, Kohlberger T, Schnörr C, Nobach H (2005) Variational optical flow estimation for particle image velocimetry. Exp Fluids 38(1):21–32

Rutgers MA, Wu XL, Bhagavatula R, Petersen AA, Goldburg WI (1996) Two dimensional velocity profiles and laminar boundary layers in flowing soap films. Phys Fluids 8(11):2847–2854

Rutgers MA (1998) Forced 2d turbulence: experimental evidence of simultaneous inverse energy and forward enstrophy cascades. Phys Rev Lett 81:2244–2247

Samanta D, Ingremeau F, Cerbus R, Tran T, Goldburg WI, Chakraborty P, Kellay H (2014) Scaling of near wall flows in quasi-two-dimensional turbulent channels. Phys Rev Lett 113(2):024504

Settles GS (2001) Schlieren and shadowgraph techniques. Experimental fluid mechanics, 1st edn. Springer, Berlin Heidelberg

Sosa R, Arnaud E, Memin E, Artana G (2006) Schlieren image velocimetry applied to ehd flows. In: Proc. of the Int. Symposium on Electrohydrodonamics (ISEHD), pp 331–334

Tong P, Goldburg WI, Chan CK, Sirivat A (1988) Turbulent transition by photon-correlation spectroscopy. Phys Rev A 37:2125–2133

Tran T, Chakraborty P, Gioia G, Steers S, Goldburg W (2009) Marangoni shocks in unobstructed soap-film flows. Phys Rev Lett 103(10):104501

Trapeznikov AA (1957) Application of the method of two-dimensional viscosity and shear strength to the investigation of the structure and composition of two-sided films and surface layers in solutions of soaps and saponins. In: Proceedings of the Second International Congress on Surface Activity, Butterworths, London

Vorobieff P, Rivera M, Ecke RE (2001) Imaging 2d turbulence. J Vis 3(4):323–330

Wang B, Cai Z, Shen L, Liu T (2015) An analysis of physics-based optical flow. J Comput Appl Math 276:62–80

Weiss J (1991) The dynamics of enstrophy transfer in two-dimensional hydrodynamics. Phys D Nonlinear Phenom 48(2):273–294

Wu Y, Fu S, Xing HJ, Kothari R (2000) Flow visualization using the negative-positive grid schlieren system and its image analysis. In: The 9th (Millennium) Symposium on Flow Visualization, Edinburg

Yang TS, Wen CY, Lin CY (2001) Interpretation of color fringes in flowing soap films. Exp Therm Fluid Sci 25(34):141–149

Zdravkovich MM (1977) Review of flow interference between two circular cylinders in various arrangements. J Fluids Eng 99(4):618–633

Zdravkovich MM (1985) Flow induced oscillations of two interfering circular cylinders. J Sound Vib 101(4):511–521

Zhong JQ, Jun Z (2005) Thermal convection with a freely moving top boundary. Phys Fluids 17(11):1–12